

Interlayer Charge-density-wave Vector Phase Induced Structural Chirality

Sen Shao,^{1,*} Wei-Chi Chiu,^{2,3,*} Tao Hou,¹ Naizhou Wang,¹ Ilya Belopolski,⁴ Yilin Zhao,¹ Jinyang Ni,¹ Qi Zhang,⁵ Yongkai Li,^{6,7,8} Jinjin Liu,^{6,7,8} Mohammad Yahyavi,¹ Yuanjun Jin,¹ Qiange Feng,^{1,9} Peiyuan Cui,¹ Cheng-Long Zhang,¹⁰ Yugui Yao,^{6,7} Zhiwei Wang,^{6,7,8} Jia-Xin Yin,⁹ Su-Yang Xu,¹¹ Qiong Ma,^{12,13} Wei-bo Gao,¹ Md Shafayat Hossain,¹⁴ Arun Bansil,^{2,3,†} and Guoqing Chang^{1,‡}

¹*Division of Physics and Applied Physics, School of Physical and Mathematical Sciences, Nanyang Technological University, 21 Nanyang Link, 637371, Singapore*

²*Department of Physics, Northeastern University, Boston, MA 02115, USA*

³*Quantum Materials and Sensing Institute, Northeastern University, Burlington, MA 01803, USA*

⁴*RIKEN Center for Emergent Matter Science (CEMS), Wako, Saitama 351-0198, Japan*

⁵*Laboratory for Topological Quantum Matter and Advanced Spectroscopy (B7), Department of Physics, Princeton University, Princeton, New Jersey 08544, USA*

⁶*Centre for Quantum Physics, Key Laboratory of Advanced Optoelectronic, Quantum Architecture and Measurement (MOE), School of Physics, Beijing Institute of Technology, Beijing 100081, China*

⁷*Beijing Key Lab of Nanophotonics and Ultrafine Optoelectronic Systems, Beijing Institute of Technology, Beijing 100081, China*

⁸*Material Science Center, Yangtze Delta Region Academy of Beijing Institute of Technology, Jiaxing 314011, China*

⁹*Department of Physics, Southern University of Science and Technology, Shenzhen, Guangdong 518055, China*

¹⁰*Beijing National Laboratory for Condensed Matter Physics, Institute of Physics, Chinese Academy of Sciences, Beijing 100190, China*

¹¹*Department of Chemistry and Chemical Biology, Harvard University, Cambridge, MA, USA*

¹²*Department of Physics, Boston College, Chestnut Hill, MA, USA*

¹³*CIFAR Azrieli Global Scholars program, CIFAR, Toronto, Canada*

¹⁴*Department of Materials Science and Engineering, University of California, Los Angeles, California, 90095 USA*

(Dated: March 13, 2026)

Chiral charge density waves (CDWs) have attracted intense interest due to their exotic quantum properties, yet the microscopic origin of structural chirality emerging from correlated charge order remains elusive. Here, we reveal that the interlayer phases of CDW wave vectors, an overlooked degree of freedom, play a crucial role in driving chiral structural displacements in layered CDW materials. By explicitly incorporating the interlayer phases in first-principles calculations, we successfully obtained the chiral structure of the CDW phases of AV_3Sb_5 ($A = K, Rb, \text{ and } Cs$) and $1T-TiSe_2$. The electronic and optical properties of the predicted chiral structures are consistent with experimental measurements of these materials in their CDW phases. We further predict that $1T-NbSe_2$ is a promising material candidate for realizing chiral CDW order. Beyond materials prediction, our theory reveals that the chiral CDW can be manipulated by electron filling. Our study opens new avenues for discovering, designing, and engineering chiral CDW materials.

Chirality, a fundamental geometrical property, plays a pivotal role in understanding a wide range of exotic phenomena in condensed matter systems [1–18]. A notable example is a chiral charge density wave (CDW), where chirality arises from a correlated charge order [19–30]. In $1T-TiSe_2/1T-TaS_2$, fast electrical and optical control and manipulation of chirality have been realized in the chiral CDW phases [22–27]. Recent studies of AV_3Sb_5 ($A = K, Rb, Cs$) have further demonstrated that chiral CDWs can support unconventional properties in transport, optics, and superconductivity [28–31]. Despite significant research interest, the mechanism behind chirality arising from correlated charge orders remains elusive [19–21, 32–37].

A central challenge lies in clarifying the relationship between chiral CDWs and structural chirality. For instance, while recent experiments on CsV_3Sb_5 reveal that its chiral CDW phase is structurally chiral [32], first-

principles calculations indicate its energetically stable CDW structures to be achiral [33–35]. Earlier studies suggested that assigning different phases ϕ_i to the three inequivalent bulk CDW wave vectors \mathbf{Q}_i , describing atomic displacements as $\mathbf{u}_i(\mathbf{R}) = u_0 \boldsymbol{\varepsilon}_i \cos(\mathbf{Q}_i \cdot \mathbf{R} + \phi_i)$, can generate a helical charge pattern [Fig. 1(a)][19]. While such phase arrangements can produce charge chirality, they necessarily break crystal symmetries within each layer (e.g., inversion, C_3 rotation, and certain mirror planes). In contrast, first-principles calculations on these known chiral CDW materials show that thermodynamically stable configurations emerge only when all symmetry-equivalent triple- \mathbf{Q} components are incorporated within each layer [33, 34].

This discrepancy between theoretical modeling, first-principles calculations, and experimental observations hinders the discovery of new chiral CDW materials. Consequently, only a handful of materials are currently

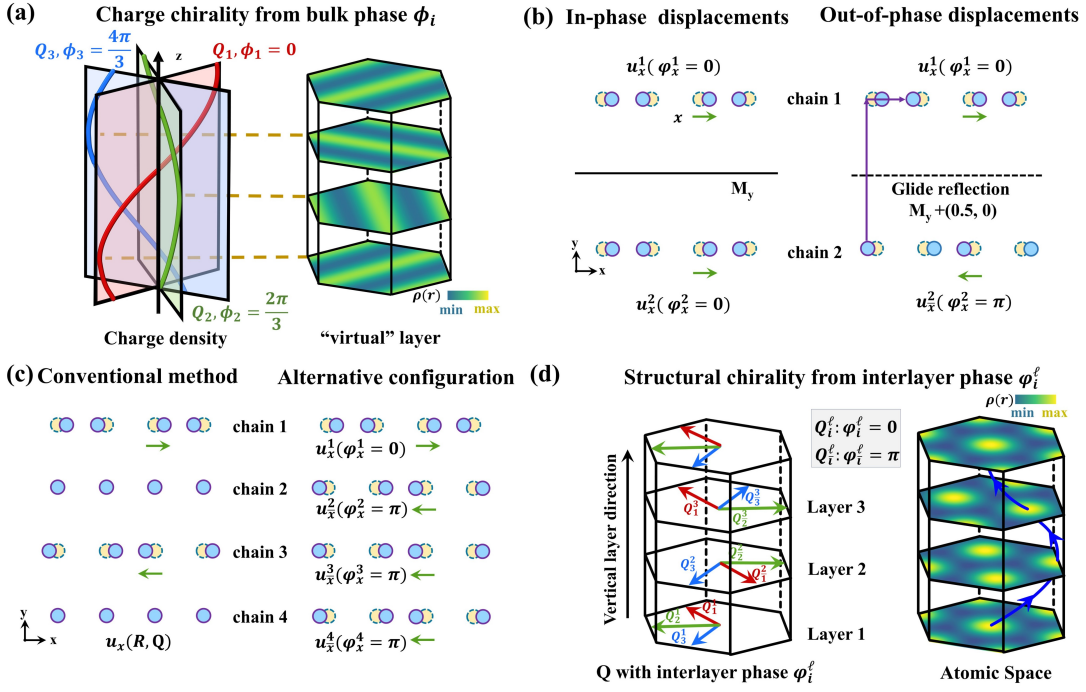


FIG. 1. (a) Left: Charge density modulation associated with each bulk wave vector \mathbf{Q}_i associated with different phases ϕ_i [19]. Right: Schematic of charge distribution in the “virtual” layer induced by different bulk wave vector phases [19]. (b) Schematic of a quasi-1D structural transition induced by in-phase and out-of-phase CDW displacements across chains. Orange and blue circles correspond to atomic positions in the original cell and the CDW cell, respectively. u_x^ℓ and u_x^r indicate opposite CDW displacements in real space, induced by $\varphi_x^\ell = 0$ and π , respectively. (c) Left: Bulk CDW wave vector $\mathbf{Q} = (\pi/x_0, \pi/2y_0)$ distorts chains 1 ($y = 0$) and 3 ($y = 2y_0$) oppositely while leaving chains 2 ($y = y_0$) and 4 ($y = 3y_0$) undistorted. Right: An alternative configuration enabled by independent interchain phase freedom with $\varphi_i^\ell = \{0, \pi, \pi, \pi\}$. (d) Left: Phase-marked interlayer wave vectors establish spiral patterns. Right: Illustration of the charge distribution at the atomic layer associated with different interlayer wave vector phases φ_i^ℓ .

known to host chiral CDWs, and all have been discovered serendipitously rather than through systematic design strategies [19, 28, 29]. To advance this rapidly emerging field, it is thus crucial to establish a theoretical framework that can achieve structural chirality that aligns with first-principles calculations and experimental observations

In this Letter, we identify a long-overlooked degree of freedom in layered CDW materials, the interlayer phases of the CDW wave vectors, which lie beyond the conventional bulk CDW description. These phases produce CDW displacements that preserve symmetry within each layer but break the overall crystal symmetry, thereby giving rise to atomic chirality. We validate this insight with first-principles calculations on kagome materials AV_3Sb_5 ($A = K, Rb, Cs$) to find a chiral structure of $2 \times 2 \times 4$ CDW phase. To demonstrate generality, we extend our predictions to the triangular-lattice materials $TiSe_2$ and $NbSe_2$. Furthermore, a minimal band picture, together with density-functional calculations, shows that electron filling tunes the competition between structure with the same and different interlayer phases configurations, enabling electrical switching of chirality.

Chiral CDW materials found in most recent studies are layered systems with weak interlayer coupling, characterized primarily by in-plane atomic displacements with negligible out-of-plane contributions [33, 38, 39]. With this in mind, we begin with one-dimensional (1D) chains exhibiting Peierls distortions along the x-direction, with weak interchain coupling along the y-direction, where each chain undergoes essentially independent in-chain displacements without out-of-chain contributions. In this scenario, adjacent chains can exhibit either in-phase displacements, resulting in a 2×1 CDW [Fig. 1(b), left], or out-of-phase displacements in opposite directions, leading to a 2×2 CDW [Fig. 1(b), right]. Here, even though each chain remains structurally equivalent, the out-of-phase CDW displacements can break crystal symmetries [Fig. 1(b)], suggesting that out-of-phase CDW displacements could be the key to understanding structural chirality in chiral CDWs.

The 2×2 CDW phase induced by out-of-phase CDW displacements can be described by a single bulk CDW wave vector $\mathbf{Q} = (\pi/x_0, \pi/y_0)$, where x_0 and y_0 are the lattice constants of the unmodulated cell. For chains located at $y = 0$ (chain 1) and $y = y_0$ (chain 2),

the atomic displacements can be written as $\mathbf{u}^1(x) = u_0 \cos(Q_x \cdot x + \phi + 0)\hat{x}$ and $\mathbf{u}^2(x) = u_0 \cos(Q_x \cdot x + \phi + \pi)\hat{x}$. Besides the global phase ϕ of \mathbf{Q} , each chain exhibits additional phases 0 and π that fix the x -direction modulations, coming from the y -direction CDW wave vector term $Q_y \cdot y_0$.

When it comes to more complex CDW displacements, the limitations of conventional bulk CDW wave vector description become apparent. For a 2×4 CDW formed by four 1D chains, the conventional approach prescribes a bulk wave vector $\mathbf{Q} = (\pi/x_0, \pi/2y_0)$. This yields atomic displacements where chains 1 ($y = 0$) and 3 ($y = 2y_0$) are distorted in opposite directions, while chains 2 ($y = y_0$) and 4 ($y = 3y_0$) exhibit no CDW distortions [Fig. 1(c), left]. However, due to the weak interchain coupling, alternative configurations of CDW displacements are allowed for 2×4 CDWs. An example is a case where chains 2, 3, and 4 all exhibit displacements opposite to those of chain 1 [Fig. 1(c), right]. Yet, such a configuration cannot be captured in the conventional bulk wave vector approach in which all phase relationships are fixed once the CDW unit cell is determined.

To incorporate this additional degree of freedom stemming from the layered nature of chiral CDW materials, we propose a generalized, layer-dependent form for the charge modulation in three-dimensional layered systems:

$$\mathbf{u}_i^\ell(\mathbf{r}^\parallel) = u_0 \varepsilon_i \cos(\mathbf{q}_i \cdot \mathbf{r}^\parallel + \phi_i + \varphi_i^\ell),$$

where ℓ indexes the layer, \mathbf{q}_i is the associated i -th CDW wave vector for the layer, \mathbf{r}^\parallel represents the in-plane atomic position within layers, and φ_i^ℓ is the additional interlayer phase shift for the i -th CDW wave vector in layer ℓ . Our key insight is that different choices of interlayer phases $\{\varphi_i^\ell\}$ introduce different CDW displacements between the layers, thereby breaking bulk inversion symmetry and giving rise to structural chirality.

To efficiently represent configurations with different interlayer phases, we define phase-tagged in-plane wave vectors that incorporate interlayer phase information: \mathbf{q}_i refers to wave vectors with $\varphi_i^\ell = 0$, while $\mathbf{q}_{\bar{i}}$ refers to those with $\varphi_i^\ell = \pi$, with \mathbf{q}_i ($\mathbf{q}_{\bar{i}}$) pointing in the positive (negative) i -direction. Consider the case of a layered CDW material with the following combination of interlayer phases configurations: $\varphi^1 = [0, 0, 0]$, $\varphi^2 = [\pi, \pi, 0]$, and $\varphi^3 = [0, \pi, \pi]$. The resulting in-plane, phase-tagged \mathbf{q} -vectors form a chiral pattern along the stacking direction [Fig. 1(d), left], corresponding to a structural chiral configuration in real space [Fig. 1(d), right].

Next, we apply the preceding approach to the real material CsV_3Sb_5 for validation using first-principles calculations. The pristine phase of CsV_3Sb_5 lies in a high-symmetry space group $P6/mmm$. Within each layer, there are two possible distorted 2×2 CDW structures: the star-of-David (SoD) and the inverse star-of-David (ISD), induced by three wave vectors Q_i ($i = 1, 2, 3$)

[33]. Accounting for all possible combinations of the associated interlayer phases configurations $[\varphi_1^\ell, \varphi_2^\ell, \varphi_3^\ell]$ yields four ISD and four SoD CDW patterns for a layer (Figs. S1-S2). As representative examples, the ISD pattern in Fig. 2(a) corresponds to the interlayer phases configuration $[0, 0, 0]$, while the pattern in Fig. 2(b), with interlayer phases configuration $[\pi, \pi, 0]$, features CDW displacements that are reversed along directions 1 and 2 relative to the reference, with direction 3 unchanged.

By systematically enumerating all inequivalent combinations of interlayer phases configurations and incorporating the corresponding structures into first-principles calculations, we find that the $2 \times 2 \times 2$ CDW phase of

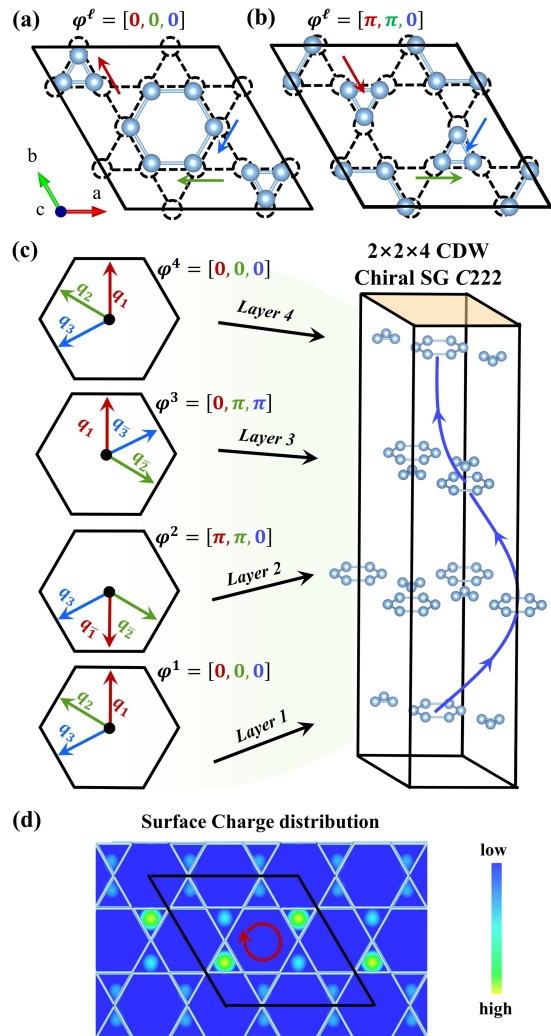


FIG. 2. (a)-(b) Inverse star-of-David patterns resulting from interlayer phases configurations $\varphi^\ell = [0, 0, 0]$ and $[\pi, \pi, 0]$, respectively. Black dashed lines represent the ideal kagome lattice. Schematic atomic displacements are denoted by red, blue, and green arrows, respectively. (c) Incorporation of interlayer wave vector phases in $2 \times 2 \times 4$ AV_3Sb_5 ($A = \text{K, Rb, and Cs}$) CDWs to induce structural chirality is illustrated. Left: Spiral phase-marked interlayer wave vector. Right: Atomic structure in the chiral space group $C222$. (d) Simulated surface charge distribution on the Sb surface.

TABLE 1. Interlayer CDW phases, and their symmetries and enthalpy differences (ΔE) relative to the pristine phases for various layered materials.

Materials	Interlayer Phases	Symmetry (Cell)	ΔE (meV/atom)
CsV ₃ Sb ₅	$\varphi^1=[0, 0, 0]$	<i>Fmmm</i>	-3.7
	$\varphi^2=[\pi, \pi, 0]$	(2×2×2)	
CsV ₃ Sb ₅	$\varphi^1=[0, 0, 0]$	<i>C222</i>	-3.7
	$\varphi^2=[\pi, \pi, 0]$		
	$\varphi^3=[0, \pi, \pi]$		
	$\varphi^4=[0, 0, 0]$		
1T-TiSe ₂	$\varphi^1=[0, 0, 0]$	<i>C2</i>	-1.2
	$\varphi^2=[0, \pi, \pi]$	(2×2×2)	
1T-NbSe ₂	$\varphi^1=[0, 0, 0]$	<i>P3₁</i>	-12.2
	$\varphi^2=[\pi, 0, 0]$		
	$\varphi^3=[\pi, \pi, 0]$		

CsV₃Sb₅ energetically favors achiral structures in the space group *Fmmm* [Table S1 in Supplementary Material (SM) [40]]. This result for the 2×2×2 CDW phase is consistent with previous studies, which show that ISD patterns have lower energy than the SoD patterns [33]. Based on this energy preference, in investigating CsV₃Sb₅ 2×2×3 and 2×2×4 supercells below, we will focus exclusively on the ISD-type CDW distortions. Our in-depth first-principles calculations encompassing all inequivalent combinations of interlayer phases configurations reveal three thermodynamically as well as dynamically stable chiral ground states: two in the 2×2×3 CDW phase and one in the 2×2×4 phase (Tables S2-S4).

We note that the 2×2×4 CDW is characterized by the combination of interlayer phases configurations $\varphi^1 = [0, 0, 0]$, $\varphi^2 = [\pi, \pi, 0]$, $\varphi^3 = [0, \pi, \pi]$, and $\varphi^4 = [0, 0, 0]$. Fig. 2(c) shows that the in-plane phase-tagged \mathbf{q} -vectors of this structure rotate along the stacking direction and drive structural chirality in the chiral space group *C222*. We obtained similar results in KV₃Sb₅ and RbV₃Sb₅ (Tables S6-S11).

Our prediction of 2×2×4 chiral structures is supported by recent X-ray photoelectron diffraction measurements that confirm the presence of chiral 2×2×4 CDW structures in CsV₃Sb₅ [32]. Furthermore, our simulated surface charge distributions exhibit spiral patterns [Fig. 2(d)] in good agreement with scanning tunneling microscopy (STM) images [28]. Additionally, circular photogalvanic effect measurements indicate that the CDW state of this family is likely to belong to the *C2* or *D2* point group [48], consistent with our predicted chiral structure in space group *C222*, which falls within the *D2* point group.

Our calculations show that the 2×2×2 achiral and 2×2×4 chiral CDW structures are nearly degenerate both in the ideal case (Tables S1,S3) and in crystals with defects (Table S5), see Table 1. This result is consistent

with experimental observations, where some experiments exclusively find the 2×2×2 phase [49], while others find the 2×2×4 phase [50], and some experiments document coexistence of these two phases [51].

We also applied our framework to consider different choices of interlayer phases φ_i^ℓ in the transition-metal dichalcogenide (TMD) 1T-TiSe₂ (Table 1). Here we obtain a stable chiral structure for 1T-TiSe₂ (Table S12), and our predicted structure matches the reported STM image (Fig. S3). [37]

Beyond predicting chiral structures in known chiral CDW materials, we investigated the triangular-lattice 1T-NbSe₂ (*P3m1*), where the 2D chiral CDW has been experimentally observed [52], but the 3D chiral CDW phase remains to be identified. Here we find that 1T-NbSe₂ exhibits $\sqrt{13} \times \sqrt{13} \times 3$ chiral CDW phase, whose combination of interlayer phases configurations is: $\varphi^1 = [0, 0, 0]$, $\varphi^2 = [\pi, 0, 0]$, and $\varphi^3 = [\pi, \pi, 0]$. Our thermodynamic and dynamic stability analyses confirm that this chiral structure is stable and energetically favorable. Thus, our calculations predict potential CDW-driven chiral phases in 3D 1T-NbSe₂ at low temperatures (Table 1, Table S13).

We emphasize that beyond predicting chiral CDW phases in layered materials, our framework also provides a pathway for tuning the chirality through electron filling. The key lies in controlling the relative interlayer phase along the z -axis. When all layers share the same CDW phase (same $[\varphi_i^\ell]$), they are translationally equivalent along the z direction [Fig. 3(a), left]. For simplicity, we use a parabolic dispersion to describe the associated band along k_z ($[-\pi/c, \pi/c]$) [Fig. 3(b), left]. When a relative CDW phase shift is introduced between the layers (different $[\varphi_i^\ell]$), the translational symmetry along z is modified and the layers become inequivalent. As an example, consider the case where the periodicity along the z -axis is doubled, leading to two inequivalent layers [Fig. 3(a), right]. To directly compare the bands of the two cases, we fold the band structure of CDW with the same $[\varphi_i^\ell]$ into an artificially doubled unit cell, where the two folded bands are degenerate at $k_z = \pi/2c$ [Fig. 3(b), left and Fig. S4]. By contrast, in the presence of different $[\varphi_i^\ell]$, the CDW modulation along z couples to the interlayer electronic degrees of freedom and lifts this degeneracy, splitting the two folded bands by pushing one upward and the other downward in energy [Fig. 3(b), right]. This splitting leads to distinct energetic consequences depending on electron filling. For example, when a single electron occupies the originally degenerate folded band point, the splitting lowers the total energy, thereby favoring the structure with different $[\varphi_i^\ell]$ [Fig. 3(b)]. In contrast, when two electrons occupy the same band point, the splitting increases the total energy, favoring the structure with the same $[\varphi_i^\ell]$ [Fig. 3(c)].

We now apply this idea to the real material CsV₃Sb₅. At the pristine Fermi level of CsV₃Sb₅, the chiral CDW

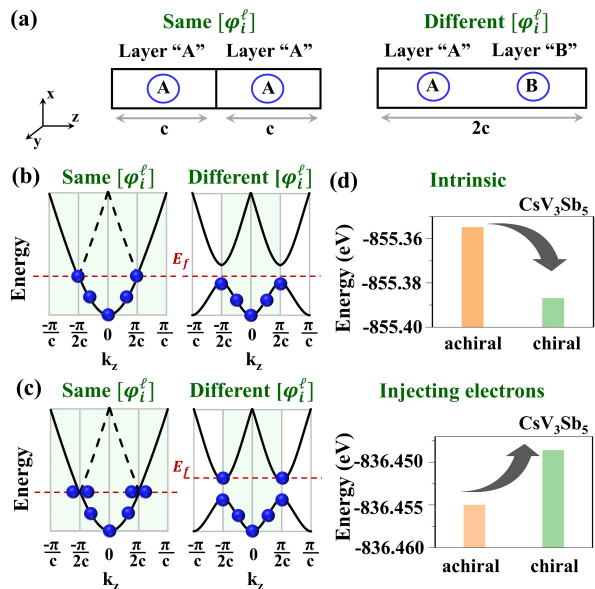


FIG. 3. (a) Left: Schematic structure with the same interlayer phase configuration ($[\varphi_i^\ell]$) along the z direction, where only layer “A” is present. Right: Schematic structure with different $[\varphi_i^\ell]$ along the z direction, where layers “A” and “B” are present. (b) Left: Schematic band for a structure with the same $[\varphi_i^\ell]$. Black solid line shows the single parabolic band along k_z in the original Brillouin zone (BZ), while the black dashed line shows its folded part in the reduced BZ, where $k_z = [-\pi/2c, \pi/2c]$. Right: A schematic band for a structure with different $[\varphi_i^\ell]$. Blue spheres denote the electron occupancy of the band. Green shadow zone represents the true BZ of the CDW structure with the same $[\varphi_i^\ell]$ (left) and different $[\varphi_i^\ell]$ (right). (c) Schematic band structures and the corresponding electron occupancies for structures with the same and different $[\varphi_i^\ell]$ in the presence of one additional electron relative to the case of panel (b). (d) Energies for achiral- $2 \times 2 \times 1$ (same $[\varphi_i^\ell]$) and chiral- $2 \times 2 \times 4$ (different $[\varphi_i^\ell]$) CsV_3Sb_5 CDW structures at the intrinsic Fermi level (top) and with the injection of three additional electrons (bottom). For comparison, we employed the same $2 \times 2 \times 4$ cell in the calculations.

structure is energetically favored over the achiral CDW structure [Fig. 3(d), top]. However, upon electron doping, specifically by introducing three additional electrons per unit cell, the energetic hierarchy reverses, and the achiral CDW structure becomes the ground state [Fig. 3(d), bottom]. Thus, the structural chirality of CsV_3Sb_5 can be switched off via electrostatic gating or chemical doping. This gate-controllable structural chirality elevates chirality to a controllable order parameter, opening a broad avenue to symmetry-programmable properties and emergent behaviors in chiral quantum matter.

Finally, we comment on the connection between the present interlayer-phase description and the standard crystallographic framework in which any modulated CDW structure can, in principle, be described through a Fourier synthesis involving an appropriate number of higher-order modulation wave vectors (Sec. X in SM). Crystallographic methods treat Fourier coefficients as

fitting parameters for post hoc structural characterization. In sharp contrast, our approach restricts interlayer phases to binary values dictated by phonon analysis—reducing the configuration space to a discrete, enumerable set to enable predictive first-principles structure searches.

By uncovering the long-overlooked interlayer phase degree of freedom in charge-density waves, an aspect that has been absent from the conventional bulk \mathbf{Q} -vector descriptions, our study bridges theory and experiment to enable systematic first-principles predictions of structurally chiral CDW materials. Moreover, our introduction of the concept of interlayer-phase-driven symmetry breaking provides a general pathway for designing and engineering new correlated CDW phases in layered materials for hosting emergent quantum phenomena.

Acknowledgements We would like to acknowledge useful discussions with F. Duncan M. Haldane. Work at Nanyang Technological University was supported by the National Research Foundation, Singapore, under its Fellowship Award (NRF-NRFF13-2021-0010), the Singapore Ministry of Education (MOE) Academic Research Fund Tier 3 grant (MOE-MOET32023-0003), and the Agency for Science, Technology and Research (A*STAR) under its Manufacturing, Trade and Connectivity (MTC) Individual Research Grant (IRG) (Grant No.: M23M6c0100).

* These authors contributed equally to this work.

† ar.bansil@northeastern.edu

‡ guoqing.chang@ntu.edu.sg

- [1] T. D. Lee, & C. N. Yang, Question of parity conservation in weak interactions, *Phys. Rev.* **104**, 254–258 (1956).
- [2] C. S. Wu, E. Ambler, R. W. Hayward, D. D. Hoppes, & R. P. Hudson, Experimental test of parity conservation in beta decay, *Phys. Rev.* **105**, 1413–1415 (1957).
- [3] G. L. J. A. Rikken, & E. Raupach, Enantioselective magnetochiral photochemistry, *Nature* **405**, 932–935 (2000).
- [4] J. B. Pendry, A chiral route to negative refraction, *Science* **306**, 1353–1355 (2004).
- [5] Y. Tang, & A. E. Cohen, Optical chirality and its interaction with matter, *Phys. Rev. Lett.* **104**, 163901 (2010).
- [6] S. Muhlbauer, *et al.*, Skyrmion lattice in a chiral magnet, *Science* **323**, 915–919 (2009).
- [7] X.-Z. Yu, *et al.*, Real-space observation of a two-dimensional skyrmion crystal, *Nature* **465**, 901–904 (2010).
- [8] G. L. J. A. Rikken, J. Fölling, & P. Wyder, Electrical magnetochiral anisotropy, *Phys. Rev. Lett.* **87**, 236602 (2001).
- [9] S. Nakatsuji, N. Kiyohara, & T. Higo, Large anomalous Hall effect in a non-collinear antiferromagnet at room temperature, *Nature* **527**, 212–215 (2015).
- [10] G. Chang, *et al.*, Topological quantum properties of chiral crystals, *Nat. Mater.* **17**, 978–985 (2018).
- [11] J. Gooth, *et al.*, Axionic charge-density wave in the Weyl semimetal $(\text{TaSe}_4)_2\text{I}$, *Nature* **575**, 315–319 (2019).

- [12] A. Szasz, J. Motruk, M. P. Zaletel, & J. E. Moore, Chiral spin liquid phase of the triangular lattice Hubbard model: a density matrix renormalization group study, *Phys. Rev. X* **10**, 021042 (2020).
- [13] Y. Liu, J. Xiao, J. Koo, & B. Yan, Chirality-driven topological electronic structure of DNA-like materials, *Nat. Mater.* **20**, 638–644 (2021).
- [14] M. Z. Hasan, *et al.*, Weyl, Dirac and high-fold chiral fermions in topological quantum matter, *Nat. Rev. Mater.* **6**, 784–803 (2021).
- [15] S.-H. Yang, R. Naaman, Y. Paltiel, & S. S. Parkin, Chiral spintronics, *Nat. Rev. Phys.* **3**, 328–343 (2021).
- [16] X. Wang, C. Yi, & C. Felser, Chiral quantum materials: when chemistry meets physics, *Adv. Mater.* **36**, 2308746 (2023).
- [17] J. Li, *et al.*, Signatures of polarized chiral spin disproportionation in rare earth nickelates, *Nat. Commun.* **15**, 7427 (2024).
- [18] C. Guo, *et al.*, Distinct switching of chiral transport in the kagome metals KV_3Sb_5 and CsV_3Sb_5 , *Nat. Commun.* **9**, 20 (2024).
- [19] J. Ishioka, *et al.*, Chiral charge-density waves, *Phys. Rev. Lett.* **105**, 176401 (2010).
- [20] J. van Wezel, Chirality and orbital order in charge density waves, *Europhys. Lett.* **96**, 67011 (2011).
- [21] B. Zenker, *et al.*, Chiral charge order in 1T-TiSe₂: Importance of lattice degrees of freedom, *Phys. Rev. B* **88**, 075138 (2013).
- [22] I. Vaskivskiy, *et al.*, Fast electronic resistance switching involving hidden charge density wave states, *Nat. Commun.* **7**, 11442 (2016).
- [23] A. Zong, *et al.*, Ultrafast manipulation of mirror domain walls in a charge density wave, *Sci. Adv.* **4**, eaau5501 (2018).
- [24] S.-Y. Xu, *et al.*, Spontaneous gyrotropic electronic order in a transition-metal dichalcogenide, *Nature* **578**, 545–549 (2020).
- [25] H. F. Yang, *et al.*, Visualization of chiral electronic structure and anomalous optical response in a material with chiral charge density waves, *Phys. Rev. Lett.* **129**, 156401 (2022).
- [26] G. Liu, *et al.*, Electrical switching of ferro-rotational order in nanometre-thick 1T-TaS₂ crystals, *Nat. Nanotechnol.* **18**, 854–860 (2023).
- [27] Y. Zhao, *et al.*, Spectroscopic visualization and phase manipulation of chiral charge density waves in 1T-TaS₂, *Nat. Commun.* **14**, 2223 (2023).
- [28] Y.-X. Jiang, *et al.*, Unconventional chiral charge order in kagome superconductor KV_3Sb_5 , *Nat. Mater.* **20**, 1353–1357 (2021).
- [29] Z. Wang, *et al.*, Electronic nature of chiral charge order in the kagome superconductor CsV_3Sb_5 , *Phys. Rev. B* **104**, 075148 (2021).
- [30] C. Guo, *et al.*, Switchable chiral transport in charge-ordered kagome metal CsV_3Sb_5 , *Nature* **611**, 461–466 (2022).
- [31] S.-Y. Yang, *et al.*, Giant, unconventional anomalous Hall effect in the metallic frustrated magnet candidate, KV_3Sb_5 . *Sci. Adv.* **6**, eabb6003 (2020).
- [32] H. J. Elmers, *et al.*, Chirality in the Kagome Metal CsV_3Sb_5 , *Phys. Rev. Lett.* **134**, 096401 (2025).
- [33] H. Tan, Y. Liu, Z. Wang, & B. Yan, Charge density waves and electronic properties of superconducting kagome metals, *Phys. Rev. Lett.* **127**, 046401 (2021).
- [34] A. Subedi, Hexagonal-to-base-centered-orthorhombic 4Q charge density wave order in kagome metals KV_3Sb_5 , RbV_3Sb_5 , and CsV_3Sb_5 , *Phys. Rev. Mater.* **6**, 015001 (2022).
- [35] B. Zhang, *et al.*, Atomistic Origin of Diverse Charge Density Wave States in CsV_3Sb_5 , *Phys. Rev. Lett.* **132**, 096101 (2024).
- [36] K. Kim, *et al.*, Origin of the chiral charge density wave in transition-metal dichalcogenide, *Nat. Phys.* **20**, 1919–1926 (2024).
- [37] H. Kim, *et al.*, Microscopic Origin of Chiral Charge Density Wave in $TiSe_2$, Preprint at <https://arxiv.org/abs/2401.01669> (2024).
- [38] S.-H. Lee, J. S. Goh, & D. Cho, Origin of the Insulating Phase and First-Order Metal-Insulator Transition in 1T-TaS₂, *Phys. Rev. Lett.* **122**, 106404 (2019).
- [39] F. Jin, *et al.*, π phase interlayer shift and stacking fault in the kagome superconductor CsV_3Sb_5 , *Phys. Rev. Lett.* **132**, 066501 (2024).
- [40] See Supplemental Material [url] for computational methods, structural information, and electronic properties, which includes Refs. [37, 41–47].
- [41] G. Kresse, & J. Furthmüller, Efficient iterative schemes for ab initio total-energy calculations using a plane-wave basis set, *Phys. Rev. B* **54**, 11169 (1996).
- [42] J. P. Perdew, K. Burke, & M. Ernzerhof, Generalized gradient approximation made simple, *Phys. Rev. Lett.* **77**, 3865 (1996).
- [43] P. E. Blöchl, Projector augmented-wave method, *Phys. Rev. B* **50**, 17953 (1994).
- [44] S. Grimme, J. Antony, S. Ehrlich, & H. Krieg, A consistent and accurate ab initio parametrization of density functional dispersion correction (DFT-D) for the 94 elements H-Pu, *J. Chem. Phys.* **132**, 154104 (2010).
- [45] Jiří Klimeš, David R. Bowler, & Angelos Michaelides, Van der Waals density functionals applied to solids, *Phys. Rev. B* **83**, 195131 (2011).
- [46] A. Togo & I. Tanaka, First principles phonon calculations in materials science, *Scr. Mater.* **108**, 1–5 (2015)
- [47] S. van Smaalen, An elementary introduction to super-space crystallography, *Z. Kristallogr. Cryst. Mater.* **219**, 681 (2004).
- [48] Z. Cheng, *et al.*, Broken symmetries associated with a Kagome chiral charge order, *Nat. Commun.* **16**, 3782 (2025).
- [49] H. Li, *et al.*, Observation of unconventional charge density wave without acoustic phonon anomaly in kagome superconductors AV_3Sb_5 ($A = Rb, Cs$), *Phys. Rev. X* **11**, 031050 (2021).
- [50] B. R. Ortiz, *et al.*, Fermi surface mapping and the nature of charge-density-wave order in the kagome superconductor CsV_3Sb_5 , *Phys. Rev. X* **11**, 041030 (2021).
- [51] Q. Xiao, *et al.*, Coexistence of multiple stacking charge density waves in kagome superconductor CsV_3Sb_5 , *Phys. Rev. Res.* **5**, L012032 (2023).
- [52] X. Song, *et al.*, Atomic-scale visualization of chiral charge density wave superlattices and their reversible switching, *Nat. Commun.* **13**, 1843 (2022).